Structure Refinement of a Cyclic Peptide from Two-Dimensional NMR Data and Molecular Modeling

Stephen W. Fesik,* Giorgio Bolis, Hing L. Sham, and Edward T. Olejniczak
Pharmaceutical Discovery Division, Abbott Laboratories, Abbott Park, Illinois 60064
Received September 4, 1986; Revised Manuscript Received December 1, 1986

ABSTRACT: The conformational and dynamic properties of a cyclic peptide designed to inhibit human renin have been examined by using NMR and molecular modeling. From a quantitative analysis of a series of two-dimensional NOE data sets, proton–proton distances were calculated. Several different methods were explored and compared to incorporate these distance constraints as well as those derived from vicinal spin–spin coupling constants into computer-generated three-dimensional structures. These methods included interactive manual manipulation of the structures to fit the NMR-determined distance constraints, distance geometry, constrained energy minimizations, and constrained molecular dynamics. The advantages and disadvantages of the methods are discussed. In addition, to gain insight into the conformations accessible to the cyclic peptide and the relative flexibility of the different parts of the molecule, molecular dynamics calculations were performed at three different temperatures. Average interproton distances and dihedral angles were obtained from the structures generated in the dynamics trajectories and compared to those obtained from the NMR experiments. Despite the four methylene groups and ether linkage contained in the cyclic portion of the peptide, our NMR results indicated a preferred conformation for the macrocyclic ring of the peptide and supported the presence of a cis Phe–Ala peptide bond. In contrast, both the molecular dynamics and NMR data indicated a considerable amount of flexibility for the remaining noncyclic portion of the molecule. These results are used to propose an explanation for the cyclic peptide's inability to inhibit human renin.

Renin, an aspartyl protease, cleaves angiotensinogen to yield angiotensin I, the precursor of the pressor octapeptide angiotensin II (Peach, 1977). Although many potent renin inhibitors have been reported (Szelke et al., 1982; Boger et al., 1983, 1985; Almquist et al., 1985), no clinically useful renin inhibitors have emerged for the treatment of hypertension. In an attempt to alleviate some of the problems associated with the known renin inhibitors (poor absorption and proteolytic instability) and give insight into the conformational properties required for renin inhibition, a series of conformationally constrained peptides were designed and synthesized (Sham et al., to be published). These peptides containing macrocyclic rings of different sizes (10, 12, and 14) were designed by fitting straight-chain peptides into an active-site model of human renin (Plattner et al., 1986) obtained from the structures of homologous aspartic proteinases (James & Sielecki, 1983; Bott et al., 1982; Pearl & Blundell, 1984; Andreeva et al., 1984) using comparative modeling techniques (Greer, 1981, 1985; Feldmann et al., 1985). On the basis of the model, the methylene groups bridging the Ala nitrogen and side chain of the adjacent residue (e.g., **1**) were predicted not to prevent

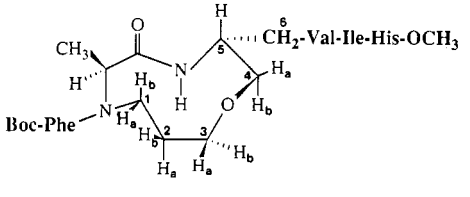

1

any important interactions in the complex nor cause any major perturbations of the enzyme. Indeed, analogues containing a 12- and 14-membered macrolide ring moderately inhibited (micromolar) both human and mouse renin. However, the 10-membered ring analogue (**1**) showed no inhibition (>100 μM) against human and mouse renin (Sham et al., to be published).

Since the conformational properties of **1** may be critical in understanding this molecule's inability to inhibit renin, we have studied the three-dimensional structure and flexibility of **1** using NMR and molecular modeling. In addition to providing insight into the conformational properties necessary for renin inhibition, these studies were aimed at defining the conformational restrictions imposed by this type of chemical constraint which, although unfavorable in the case of a renin inhibitor, may be desirable for other peptides.

Other important considerations in our work were the evaluation and development of methodologies for defining the conformational and dynamic properties of peptides. To determine highly resolved three-dimensional structures by NMR, a large number of accurate distance constraints are required. Also, computational methods are needed to generate structures based on these distance constraints that are energetically reasonable and that can be quantitatively evaluated in terms of experimentally determined parameters.

Recently, we have described methods for quantitatively analyzing two-dimensional nuclear Overhauser effect (2D NOE) data which took multispin effects into account in the data analysis (Olejniczak et al., 1986). This markedly increased both the quality and quantity of the distance constraints that could be obtained to define molecular structure (Fesik et al., 1986). Using the same methodology, we obtained many accurate proton–proton distance constraints for the cyclic peptide (**1**). These distance constraints, along with those derived from vicinal spin–spin coupling constants, were used to model three-dimensional structures of **1**.

Several different methods have recently been employed for converting NMR data into three-dimensional structures (Havel & Wüthrich, 1985; Zuiderweg et al., 1985; Clore et al., 1985; Fesik et al., 1986). In this work, we compared several of these

* Correspondence should be addressed to this author.

0006-2960/87/0426-1851$01.50/0

approaches for converting the distance constraints obtained for **1** into a three-dimensional structure. These included (1) interactive manual manipulation of computer-generated structures to fit the NMR-determined distance constraints, (2) energy minimization using molecular mechanic force fields containing an extra term of the form $K(r - r_0)^2$ used to constrain the interproton distances (r) to the distances (r_0) determined experimentally, (3) constrained molecular dynamics, and (4) distance geometry. The strengths and weaknesses of each method in generating a structure of the constrained peptide **1** are discussed.

In addition, information on the relative flexibility for the different parts of the peptide analogue was obtained from an analysis of a series of molecular dynamics trajectories run at three different temperatures. These results along with the NMR data were able to provide a detailed description of both the structural and dynamic behavior of the constrained cyclic peptide.

Experimental Procedures

NMR. NMR samples (25 mM) of the cyclic peptide were prepared in dimethyl-d_6 sulfoxide (Me_2SO-d_6)/H_2O and Me_2SO-d_6/D_2O in a 2/1 (v/v) ratio. These solvent conditions were employed to increase the viscosity of the solution in order to increase the magnitude of the observed NOEs.

NMR spectra were recorded at 30 °C on a General Electric GN-500 NMR spectrometer and processed by using the Fourier transform (FT) NMR program of Dr. D. Hare. Correlated spectroscopy (COSY) (Aue et al., 1976) experiments were acquired with a (90°–t_1–90°–acquire)$_n$ pulse sequence and processed in the absolute-value mode by using a sinebell window function in each dimension before Fourier transformation. The 2D NOE experiments were performed by using a (90°–t_1–90°–Υ_m–90°–acquire)$_n$ pulse sequence with a phase cycling scheme designed to separate the real and imaginary parts of the t_1 dimension (States et al., 1982). No attempt was made to suppress zero quantum coherence evolving during the Υ_m period (Macura et al., 1982), since these effects had only a minor, if any, contribution to the overall cross-peak volumes for the mixing times used. For the peptide analogue in Me_2SO-d_6/D_2O, six 2D NOE data sets (256 × 4K) were collected with mixing times (Υ_m) of 50, 100, 200, 300, 400, and 700 ms using a delay of 2.2 s between scans. Two 2D NOE data sets (512 × 4K) with mixing times of 100 and 250 ms were collected for the peptide analogue in Me_2SO-d_6/H_2O.

For processing the 2D NOE data sets, the free induction decays were multiplied by a cosine window function, Fourier transformed, and phase corrected in ω_2. The complex time domain data in the t_1 dimension were assembled from the extracted real parts of the two sets of Fourier-transformed spectra as previously described (States et al., 1982), multiplied by a cosine window function, zero filled, Fourier transformed, and base-line corrected in ω_1 using a fifth-order polynomial.

The cross-peak and diagonal peak volumes necessary for the calculations of interproton distances were measured from the unsymmetrized 2D NOE data sets by summing over all the data points within a particular radius. To facilitate this laborious task, computer programs were written to automatically pick the peaks of interest for the entire series of 2D NOE data sets, integrate their volumes, and store the data in a matrix suitable for the interproton distance calculations. As described in detail elsewhere (Olejniczak et al., 1986), proton–proton distances were calculated from the volume matrix, $V(\Upsilon_m)$, of cross-peak and diagonal peak volumes by first solving for the relaxation rate matrix, R, using

$$V(\Upsilon_m) = e^{-R\Upsilon_m}V^0 \quad (1)$$

where V^0 is the volume at $\Upsilon_m = 0$ (Bremer et al., 1984; Perrin & Gipe, 1984; Olejniczak et al., 1986). From the cross-relaxation rates (σ) extracted from R and a known distance (r_{kl}), unknown distances (r_{ij}) were calculated with the assumption that the dynamics of both nuclear vectors are the same (Noggle & Shirmer, 1972) using the equation:

$$r_{ij} = \left[r_{kl}^6 \frac{\sigma_{kl}}{\sigma_{ij}} \right]^{1/6} \quad (2)$$

Our known distance was chosen to be the distance (1.78 Å) between the geminal protons of the macrocyclic ring. Unlike most geminal proton pairs in proteins, the NOE cross-peaks in this case were well separated from the diagonal, allowing an accurate measure of their volumes.

Computational Methods. Initial structures were created by using standard bond lengths and bond angles. Calculations and graphics were performed on a Vax 785 computer which served as the host for the Evans and Sutherland picture system and for a FPS-164 array processor.

Energy minimizations and dynamics calculations were performed by using the valence force field (VFF) program of A. T. Hagler (Hagler et al., 1979; Lifson et al., 1979) which treats all of the hydrogens of the system explicitly. The parameters used in the calculations were those supplied by the program except for the charge on the valine nitrogen which was reduced to approximate the screening effect of solvent which was not included in the calculations.

The standard empirical potential function described by Hagler et al. (1985) was employed. For the constrained minimizations and dynamics, an extra harmonic term of the form $K(r - r_0)^2$ was added to constrain the interproton distances (r) to the experimentally determined distances (r_0). The value of K was chosen on the basis of the accuracy of the measured distances, r_0, using the equation:

$$K = \frac{kTC}{2(\Delta ij)^2} \quad (3)$$

where k = the Boltzmann constant, T = the temperature (in degrees kelvin), C = the scale factor, and Δij = the estimated error in NMR-determined distances between protons i and j. In most cases, a value of $C = 1$ was chosen which corresponds to force constants (K) of 0.5–7.5 kcal mol^{-1} Å^{-2}, depending on Δij. In some of the constrained energy minimizations, K was scaled up by increasing C to a maximum value of 50 kcal mol^{-1} Å^{-2} in an attempt to more heavily weight the NMR constraints. For the constrained molecular dynamics calculations, an additional equilibration period was included to account for the initial heating caused by the additional terms in the potential function.

Several structures were also generated by using a distance geometry algorithm supplied by Prof. I. D. Kuntz (Havel et al., 1983). All distances fixed by the covalent bonding of the molecule were used as input. This included distances fixed by one and two covalent bonds as well as upper and lower bounds for four atoms connected by three covalent bonds. Lower bounds for nonbonded atom pairs were always greater than or equal to the sum of the van der Waals radii of the atoms. Nine chirality constraints were employed in the optimization to eliminate structures with incorrect stereochemistry, and five additional constraints were included to keep the peptide bonds planar. All sp_2 carbons and their substituents were also kept planar. In addition to these constraints de-

Table I: Proton Chemical Shift Assignments (ppm) of **1** in Me_2SO-d_6/H_2O and Me_2SO-d_6/D_2O (2/1)[a]

proton	ppm	proton	ppm	proton	ppm
His NH	8.39	4a	3.80	6a	2.53
Ile NH	8.01	CO_2CH_3	3.62	6b	2.39
ring NH	7.74	3a	3.51	2a	2.12
His ϵ_1	7.59	1a	3.24	Val β	1.83
Phe NH	7.57	3b	3.02	Ile β	1.74
Phe ring	7.32–7.20	His β	3.00	2b	1.57
His δ_2	6.85	Phe β	2.94	Boc CH_3	1.39
Phe α	4.81	His β	2.93	Ile γ	1.30
Ala α	4.75	Phe β	2.86	Ile γ	1.05
His α	4.49	4b	2.79	Val CH_3	0.85
Ile α	4.21	Val α	2.78	Ile γCH_3	0.82
5	4.16	1b	2.69	Ile δCH_3	0.80
				Ala CH_3	0.30

[a] Chemical shifts are reported relative to tetramethylsilane.

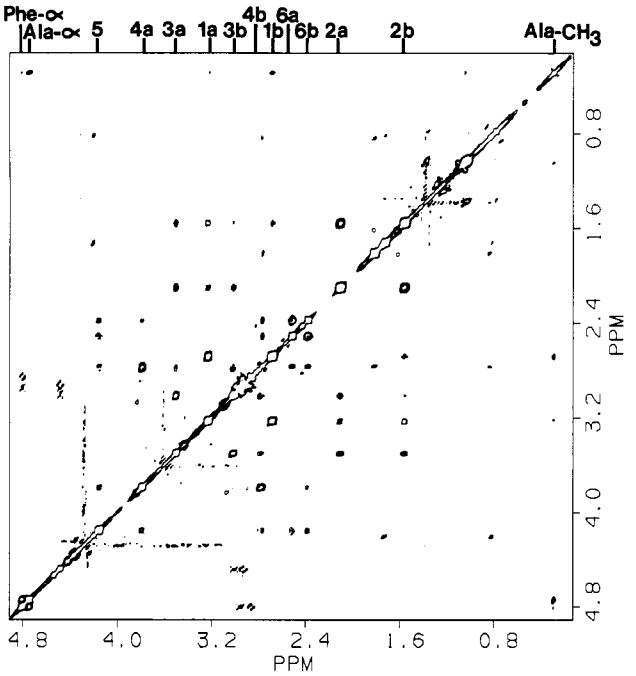

FIGURE 1: Portion of a two-dimensional NOE contour map of **1** obtained in Me_2SO-d_6/D_2O at 500 MHz. The assignments of the protons of the macrocyclic ring are given at the top of the plot.

termined by the covalent bonding, 37 constraints were obtained from the NMR data, including 21 accurate (±0.2 Å) interproton distances defining the cyclic portion of the peptide plus 13 less accurate (±0.5 Å) distance constraints describing the remainder of the molecule. From the three large vicinal coupling constants observed for the macrocyclic ring, three additional constraints were included which fixed these protons in a trans orientation.

Results and Discussion

NMR. The proton NMR resonances of the cyclic peptide **1** were assigned (Table I) by identifying the scalar-coupled protons from COSY and the dipolar-coupled protons from 2D NOE experiments. In addition to aiding in the proton assignments, the 2D NOE experiments provided useful conformational information. For example, as shown in Figure 1, NOE cross-peaks were observed between the αCH of the Phe and Ala residues, indicating their close proximity. These results suggested the presence of the cis Phe–Ala peptide bond. NOEs between the Phe ring and Ala CH_3 protons (data not shown) indicated the close proximity of these protons and were consistent with the upfield ring current shift (0.3 ppm) observed for the Ala CH_3 protons. The conformation of the

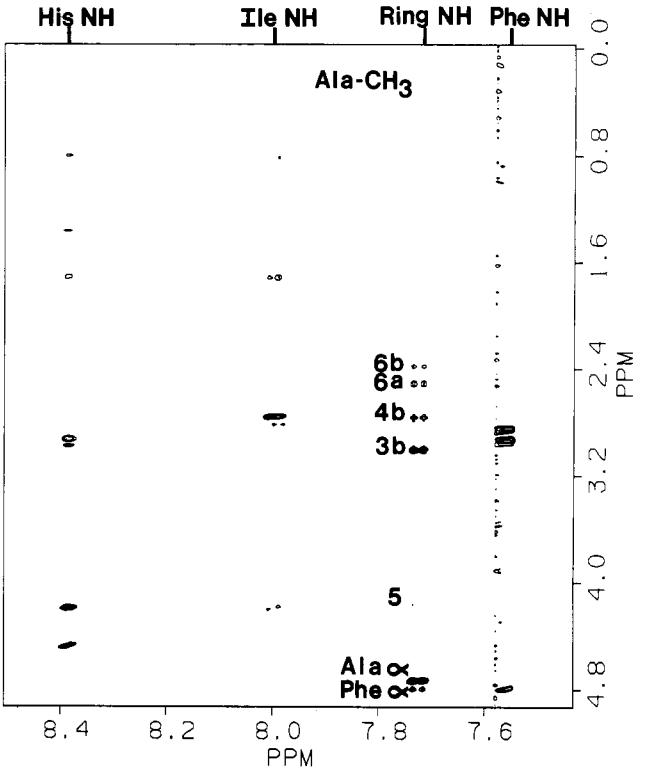

FIGURE 2: Portion of a two-dimensional NOE contour map of **1** obtained in Me_2SO-d_6/H_2O. The labels indicate the assignments of the NH protons and the expected locations of NOE cross-peaks between the ring NH and other protons of the molecule.

macrocyclic ring was defined by NOEs between the ring protons observed in Me_2SO-d_6/D_2O and Me_2SO-d_6/H_2O. As depicted in the 2D NOE contour map of Figure 2, NOEs between the NH proton of the macrocyclic ring and the αCH of Ala and Phe indicated that the ring NH was located on the same side of the ring as the αCH of Ala. This conformation of the macrocycle would position the NH on the opposite side of the ring as the Ala CH_3 and 5-proton which was consistent with the lack of NOEs observed between the ring NH and these protons (Figure 2). Additional NOEs between the ring NH and 3b, 4b, 6a, and 6b ring protons defined the relative spatial relationship of these protons and provided further information on the conformation of the macrocyclic ring.

To probe the conformation of **1** in a more detailed manner, accurate proton–proton distances (Table II) were calculated from a multispin analysis of the cross-peak and diagonal peak volumes obtained from a series of 2D NOE data sets acquired with different mixing times. Figure 3 depicts representative examples of the NOE data, including simulations based on the relaxation matrix obtained from the measured cross-peak and diagonal peak volumes. Since multispin effects were taken into account in the data analysis, the major source of error in the proton–proton distances was due to inaccurate volume integrations. The errors reported were estimated from the differences in the relaxation constants determined from the six different mixing times. The error bars were increased if the simulations based on these relaxation rates did not give a good fit to the actual data.

Accurate distance constraints are very important to define detailed molecular structures, especially for distances between protons on adjacent carbons. In this case, the possible proton–proton distances are from 2.3 to 3.1 Å for an eclipsed to anti conformation, respectively. Thus, if the distances can only be determined to an accuracy of ±0.5 Å, then the conformation cannot be defined.

Table II: Proton–Proton Distances Obtained Experimentally from 2D NOE Experiments Compared to Distances Measured from Computer-Generated Structures[a,b]

	distances (Å)				
	from	structure	dynamics		
proton–proton[c]	NOE	I	300 K	500 K	800 K
1a–2a	2.4	2.42	2.42	2.44	2.42
1a–2b	2.5	2.47	2.48	2.47	2.48
1b–2a	3.1	3.06	3.06	3.07	3.00
1b–2b	2.5	2.40	2.40	2.41	2.41
1b–3b	3.3	3.40	3.43	3.42	3.45
2a–3a	2.3	2.40	2.41	2.41	2.42
2a–3b	2.4	2.51	2.51	2.51	2.55
2b–3a	2.5	2.50	2.50	2.51	2.53
2b–3b	2.9	3.08	3.08	3.08	3.08
3a–4b	2.7	2.75	2.78	2.82	2.87
3b–4b	2.3	2.31	2.32	2.34	2.36
4a–5	2.5	2.43	2.44	2.44	2.44
4b–5	2.9	3.09	3.09	3.09	3.10
ring NH–4b	2.8	2.69	2.72	2.64	2.70
ring NH–3b	2.5	2.38	2.54	2.47	2.55
5–6(a,b)	2.7	2.91	2.67	2.70	2.45
5–6(a,b)	2.8	2.96	3.11	3.08	2.41
4a–6(a,b)	2.7	2.54	2.47	2.47	3.69
4b–6(a,b)	2.4	2.30	2.66	2.68	3.66
4b–6(a,b)	2.3	3.16	2.70	2.84	2.70
ring NH–6a	2.7	3.43	3.73	3.67	3.25
ring NH–6b	2.8	2.67	2.63	2.76	3.83
Ala CH_3–1a	3.2	3.52	3.34	3.57	3.60
Ala CH_3–1b	2.9	3.12	3.12	3.16	3.14
Ala α–Phe α	1.8	2.03	2.01	2.04	2.08
Ile NH–Val α	2.4	2.18	2.19	2.14	2.23
His NH–Ile α	2.8	2.14	2.17	3.57	2.29

[a] Average proton–proton distances ($\langle r \rangle$) were calculated from the distances (r) measured from the structures generated in the dynamics using $\langle r \rangle = [(1/N)\sum_{i=1}^{N}(1/r_i^6)]^{-1/6}$. [b] Effective distances to the methyl groups were calculated from the approximation $r = [(1/3)\sum_{i=1}^{3}(1/r_i^6)]^{-1/6}$. [c] Protons 6a and 6b were not stereospecifically assigned.

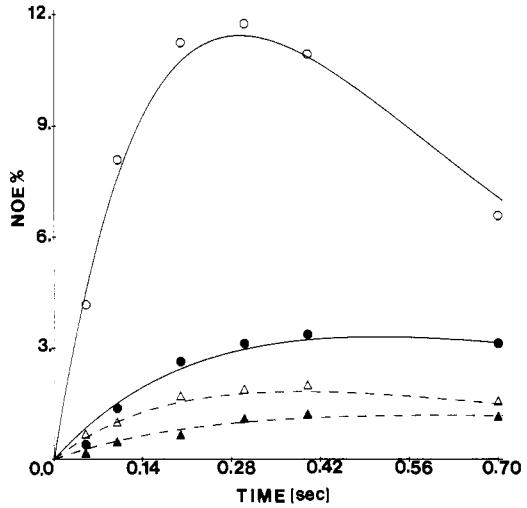

FIGURE 3: Experimental two-dimensional NOE data [(○) 2a–2b; (●) 4b–6b; (△) 2a–3b; (▲) 4a–6a] compared to multispin simulations based on the relaxation matrix obtained from the measured cross-peak and diagonal peak volumes (eq 1).

Interactive Model Building and Energy Minimization. To obtain an energetically favorable structure that was consistent with the NMR data, we needed to generate a computer model of the cyclic peptide **1** and subsequently evaluate its conformational energy. Upon generating an initial structure based on standard bond lengths and angles, we attempted to interactively modify this structure to agree with the NMR data. This was accomplished by manually rotating about covalent bonds, satisfying one distance constraint at a time. The resulting structure changed very little upon energy minimization (root mean square = 0.39 Å for Phe and ring atoms) which merely removed energetically unfavorable steric interactions. Figure 4 depicts the structure of **1** that was obtained in the above-mentioned manner. Although most of the proton–proton distances and dihedral angles of this structure compared favorably to those obtained from the NMR data (Tables II and III), some of the data did not fit and was best explained by considering an average structure as will be described later (Molecular Dynamics). Furthermore, we found several disadvantages of this method. One of the major problems was the difficulty of maintaining all of the distance constraints simultaneously. In our attempts to satisfy the distance constraints for one portion of the molecule, some of the previously imposed distance constraints were no longer satisfied. In addition, using this approach, it is difficult to evaluate the uniqueness of the structures that are generated; i.e., could other structures fit the NMR data equally well? Finally, the method requires biased user interaction; thus, less biased and more automated methods would be preferable.

Table III: Dihedral Angles Obtained Experimentally from Vicinal Spin–Spin Coupling Constants Compared to Dihedral Angles Measured from Computer-Generated Structures[a,b]

		dihedral angles				
	J	from J	structure	dynamics		
protons[c]	(Hz)	values[d]	I	300 K	500 K	800 K
1a–2a	5.5	44 (125)	51	51	52	51
1a–2b	2.5	68 (103)	61	62	60	58
1b–2a	10.8	157	162	161	162	158
1b–2b	5.4	45 (125)	50	49	50	49
2a–3a	4.2	53 (118)	50	51	50	50
2a–3b	≤1.5	80–100	65	107	107	109
2b–3a	3.5	59 (113)	63	62	62	60
2b–3b	10.0	151	178	175	175	168
4a–5	5.1	47 (123)	52	52	57	55
4b–5	11.3	161	167	167	170	168
ring NH–5	10.1	164	163	167	156	158
5–6(a,b)	6.7	36 (132)	118	78	71	44
5–6(a,b)	6.0	41 (128)	127	164	155	55
Phe NH–α	6.7	132 (36)	166	147	149	153
Ile NH–α	9.0	155	170	149	139	151
His NH–α	7.3	144 (24)	173	156	154	148
Phe α–β	6.0	41 (128)	70	69	67	40
Phe α–β	10.0	151	176	172	172	139
His α–β	5.5	44 (125)	64	52	67	45
His α–β	8.6	143 (20)	179	149	168	120
Ile α–β	7.4	31 (136)	51	59	62	62

[a] Assumes a Karplus equation of the form $J = 9.4\cos^2\theta - 1.1\cos\theta + 0.4$ for the J_{NH}, αCH coupling constants and $J = 9.4\cos^2\theta - 1.4\cos\theta + 1.6$ for the side chains (Bystrov, 1976). [b] Average dihedral angles were calculated by averaging the J couplings for each of the structures obtained from the dynamics followed by the conversion to the dihedral angles using the appropriate Karplus equation. [c] Protons 6a and 6b were not stereospecifically assigned. [d] The sign of the dihedral angle cannot be determined from the measured coupling constant.

Constrained Energy Minimization. Another method which has recently been reported for converting NMR data into structures is constrained energy minimization (Clore et al., 1985; Fesik et al., 1986). In this method, an extra term is added to the force field to constrain the interproton distances to those determined experimentally (see Experimental Procedures). Although successful in some cases for producing structures that agree with the NMR data, Clore and coworkers (Clore et al., 1985) have shown that for oligonucleotides the convergence properties of constrained energy minimization are dependent on the starting structure. To test the convergence properties of this method using the cyclic peptide, three different starting structures (C1, C2, and C3) were subjected to constrained energy minimizations. These

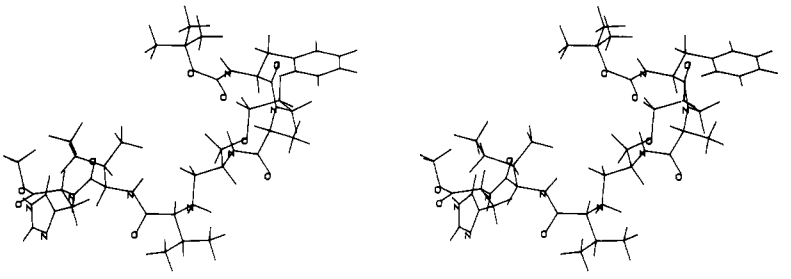

FIGURE 4: Stereoview of the structure (C1) generated by manually rotating about covalent bonds to agree with the NMR data.

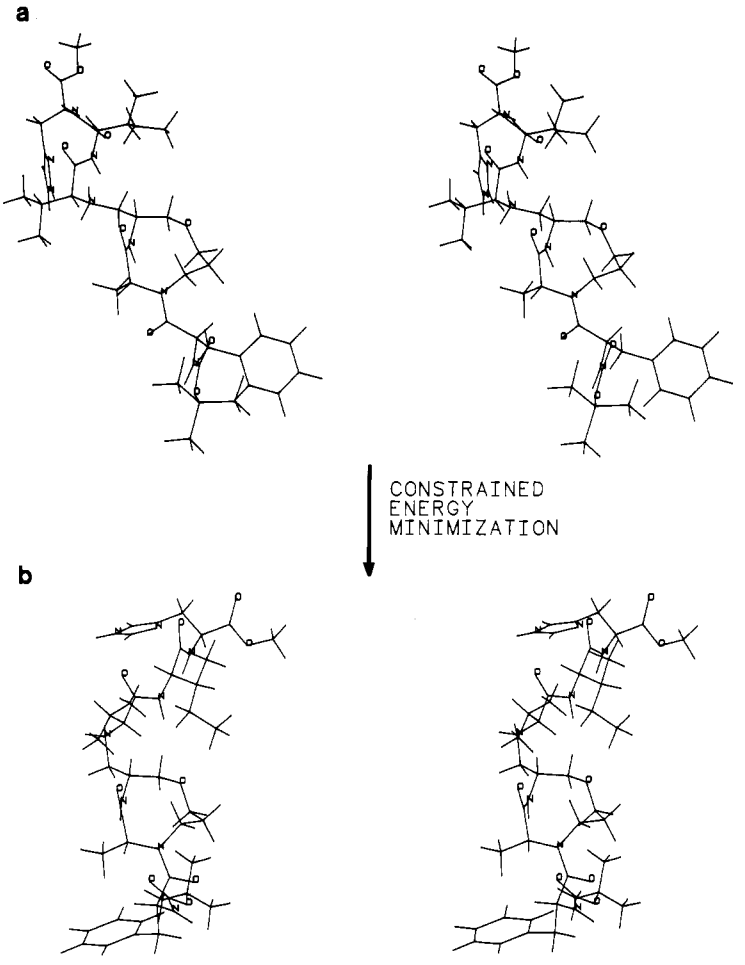

FIGURE 5: (a) Stereoview of **1** containing a trans Phe–Ala peptide bond. (b) Structure with cis conformation in which an extra term, $K(r - r_0)^2$, was added to the potential function to constrain the interproton distances (r) to the experimentally determined distances (r_0).

included the structure depicted in Figure 4 (C1) as well as structures which did not fit the NMR data (C2 and C3). Both structures C2 and C3 differ from C1 by having a trans Phe–Ala peptide bond. In addition, the 5–4–O–3 dihedral angle in the ring of C3 is 180° different from that of the corresponding angles in C1 and C2, resulting in a significantly different ring pucker. As shown in Figure 5, using the starting structure, C2, containing the trans Phe–Ala peptide bond, constrained energy minimization was successful in producing a structure with a cis Phe–Ala peptide bond, consistent with the NMR data. In contrast, constrained energy minimizations did not allow the convergence to the same structure starting from the cyclic peptide structure, C3, even when a relatively high force constant (K = 50 kcal mol^{-1} Å^{-2}) was employed as part of the extra term of the potential function. If even higher force constants are employed, this last term begins to outweight the energy terms corresponding to the bond lengths and bond angles causing the structure to be distorted. Thus, constrained energy minimization does not have good convergent properties due to its inability to overcome local energy minima and is therefore an unsatisfactory method for generating structures from NMR data unless the starting structure used as input is close to the final optimum structure.

Constrained Molecular Dynamics. Another method that has recently been applied in the refinement of structures using NMR data is constrained molecular dynamics (Zuiderweg et al., 1985; Kaptein et al., 1985; Clore et al., 1985). Using this approach, we performed molecular dynamics calculations using a potential energy function that contained the same additional term which was applied in constrained energy minimization. Unlike constrained energy minimization, however, constrained molecular dynamics had a greater capacity of overcoming energy barriers between local minima due to the kinetic energy available in the calculations. Indeed, all of the starting structures (C1, C2, and C3) converged to structures consistent with the NMR data. For example, as shown in Figure 6, a structure similar to C1 (root mean square = 0.23 Å for ring and Phe atoms) was produced from a starting structure con-

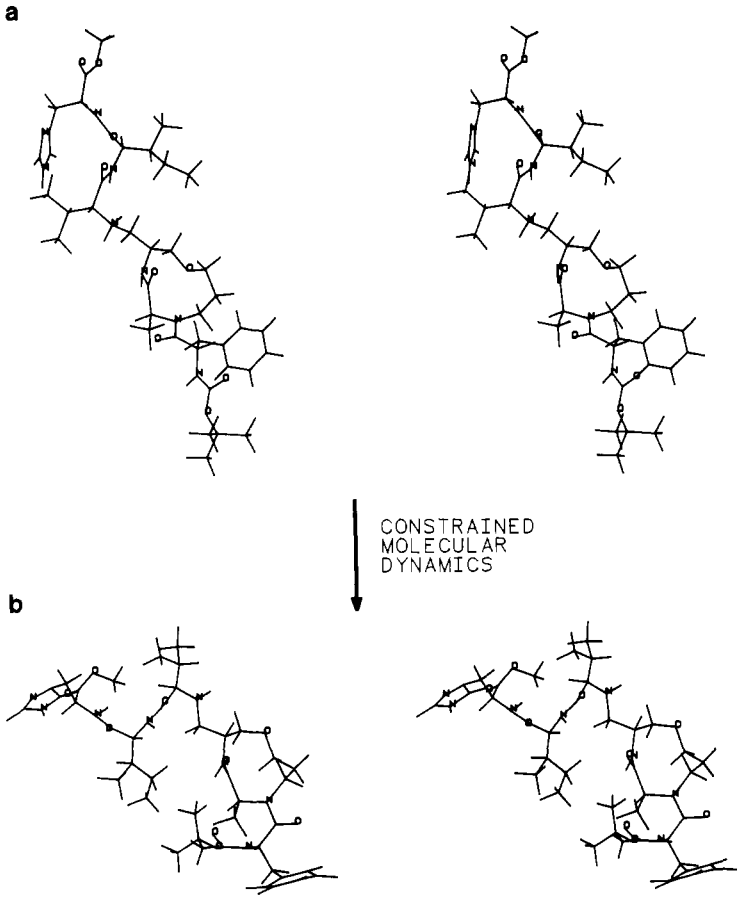

FIGURE 6: (a) Stereoview of **1** containing a trans Phe–Ala peptide bond and a different macrocyclic ring pucker. (b) Structure generated that was consistent with the NMR data after constrained molecular dynamics.

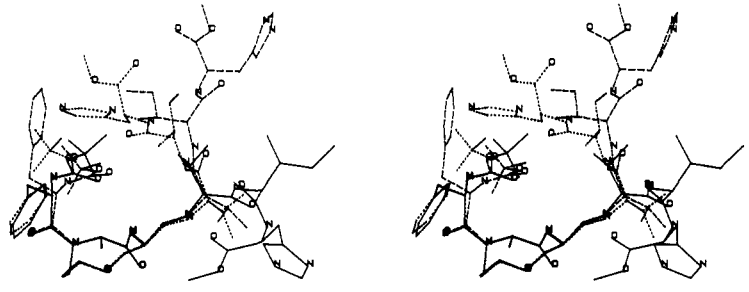

FIGURE 7: Stereoview of representative structures generated from the distance geometry algorithm after further refinement using energy minimization.

taining a Phe–Ala trans peptide bond and different macrocyclic ring pucker (C3). In our experience, the ability of the different starting structures to converge to a structure consistent with the NMR data was dependent on the value chosen for the force constant, K, as well as the temperature at which the dynamics was performed. In structure C3, for example, a small value of K (0.5–7.5 kcal mol^{-1} Å^{-2} was not enough to allow the convergence to a structure resembling C1 in the constrained dynamics performed at 300 K. Conversely, if very large force constants ($K \geq 25$ kcal mol^{-1} Å^{-2} were employed in the calculations, the structure was distorted (i.e., no longer contained the proper covalent bonds). The desired result was finally achieved by performing the constrained molecular dynamics at a higher temperature using a small force constant.

Although this method was found to be less sensitive to starting structure compared to constrained energy minimization for the small peptide used in these studies, it might be expected that for larger molecules in which larger energy barriers must be crossed to produce global structural changes, suitable starting structures are a necessity. This was found to be the case in structural studies of the *lac* repressor headpiece (Zuiderweg et al., 1985). The conformation of the backbone determined from constrained molecular dynamics did not agree with all of the NMR data and had to be changed manually to better satisfy the NOE distance constraints (Zuiderweg et al., 1985).

Distance Geometry. Several structures were also generated from a distance geometry algorithm using distance constraints obtained from the covalent bonding and NMR data (Tables II and III). The upper and lower bounds of the distance constraints obtained from the NMR data were ±8% of the distances in Table II except for the interproton distances involving NH and CH_3 protons for which a value of ±15% was employed. As shown in Figure 7, these structures had similar conformations for the macrocyclic ring (root mean square < 0.1 Å) but differed substantially in the noncyclic portion of the peptide (root mean square = 2.5–3.5 Å), possibly reflecting the insufficient number of distance constraints for this part of the molecule. The only exception to this general rule was a structure in which the NH proton of the macrocyclic ring

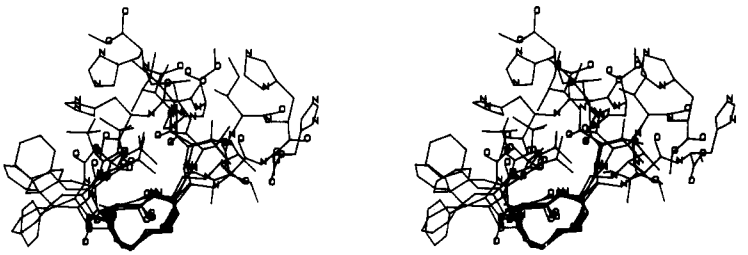

FIGURE 8: Superimposed structures which were generated at different times during a molecular dynamics trajectory performed at 800 K.

was on the same side of the ring as the Ala CH_3 and 5-proton. Although most of the NMR-determined distance constraints were satisfied in the structure which had adopted a different ring pucker, this structure was inconsistent with the lack of NOEs observed between the ring NH and Ala CH_3 and 5-proton (see Figure 2). However, when information on the protons that are *not* close in space was included in the distance geometry calculations, by increasing the lower bound between these protons to 2.7 Å, only structures containing the ring pucker of C1 were generated. These results suggest that if the lack of an observed NOE between a pair of protons is unambiguous (i.e., the location of the expected cross-peak is in a clear region of the contour map, and other NOEs to that proton are observable), then increasing the lower bounds between these protons in the distance geometry calculations can help eliminate structures inconsistent with the NMR data.

One of the distinct advantages of distance geometry is that the structures produced are unbiased by user interaction. The disadvantage is that the structures generated do not take into account bonded and nonbonded interactions and can result in energetically unfavorable structures. To relax the unfavorable interactions in the structures, energy minimization has been proposed (Williamson et al., 1985). Upon energy minimization, most of the structures generated from distance geometry remained consistent with the NMR data. However, some of the structures created by distance geometry no longer agreed with all of the experimental data after minimizing to a low-energy structure. This strategy was only successful when only slight modifications were necessary in the structure to reach a local energy minimum. These results suggest that energy refinement of starting structures created by distance geometry should include, at least initially, the experimentally determined distance constraints. This may be followed by energy minimization without the constraints.

Molecular Dynamics. To obtain information on the relative flexibility of the different parts of the cyclic peptide, molecular dynamics calculations were performed at three temperatures (300, 500, and 800 K). The calculations at the higher temperatures were performed to increase the rate of conformational interconversions and to provide insight into the conformations that may be accessible to the peptide on a longer time scale.

The results from the molecular dynamics calculations obtained at the three temperatures were initially analyzed by viewing the trajectories of the atomic coordinates on an Evans and Sutherland picture system. As illustrated in Figure 8 by the superimposed structures selected from the dynamics run at 800 K, very little change was observed in the structure of the macrocyclic ring, despite the presence of the four methylene groups and ether linkage contained in the macrocycle. Furthermore, the cis Phe–Ala peptide bond remained intact in all of the dynamics trajectories. In contrast, the peptide backbone and side chains of the Val, Ile, and His residues exhibited considerable mobility in the dynamics runs. The higher flexibility of the noncyclic portion of the peptide was also demonstrated from an analysis of the dihedral angular fluctuations exhibited in the dynamics. As shown in Figure 9, the amplitudes of the angular fluctuations that occur for representative dihedral angles from the noncyclic portion of the molecule (9B) were much greater than those of the macrocyclic ring (9A).

Due to the different time scales of the molecular dynamics (~80 ps) and NMR experiment (milliseconds) and the fact that solvent was not included in the dynamics calculations, the proton–proton distances and dihedral angles obtained from the NMR data were not expected to compare exactly to those extracted from the structures generated in the molecular dynamics calculations (Hagler, 1985). Nevertheless, it was of interest to compare the experimentally derived parameters to those calculated from the dynamics. As shown in Table II, the distances between protons of the macrocyclic ring (top of the table) obtained from the NOE experiments were nearly identical with the average distances extracted from the structures generated in the dynamics trajectories at 300 K. In addition, the average distances obtained from the dynamics were not dependent on the temperature at which the dynamics were performed. However, the standard deviation increased from ca. ±0.10 Å for those distances obtained from the dynamics at 300 K to ±0.20 Å for the calculations performed at 800 K, suggesting that the amplitudes of the fluctuations are larger at the higher temperatures but occur about a single conformation of the macrocyclic ring.

Unlike the interproton distances of the macrocyclic ring, the average proton–proton distances for the noncyclic portion of the molecule obtained from the dynamics did not agree with all of the experimental data. For example, the NOE data indicate that the ring NH is almost equidistant from the 6a- and 6b-protons. Yet, the average distances obtained from the dynamics calculations at 300 K indicated that the ring NH was closer to only one of the 6-protons. This can be explained by the inability of the 5–6 bond to rotate in the 80-ps dynamics run at 300 K, resulting in the average ring NH to 6-proton distances to be similar to those obtained for the starting static structure (C1). In contrast to the dynamics performed at 300 K, rotations about the 5–6 bond did occur in the dynamics performed at 800 K, resulting in several different conformations which were reflected in the different averaged 5–6a,b dihedral angles and interproton distances. However, none of the average conformation obtained from this or any of the dynamics calculations agreed with all of the NMR data. The dynamics described here are best used to provide insight into the conformations accessible to the peptide and the relative flexibility of the different parts of the molecule.

In Table III, the average dihedral angles calculated from the structures generated in the dynamics are compared to the dihedral angles obtained experimentally from the vicinal spin–spin coupling constants. In agreement with the proton–proton distances, the dihedral angles of the macrocyclic ring calculated from the dynamics remained constant at the different temperatures and correlated well with those obtained

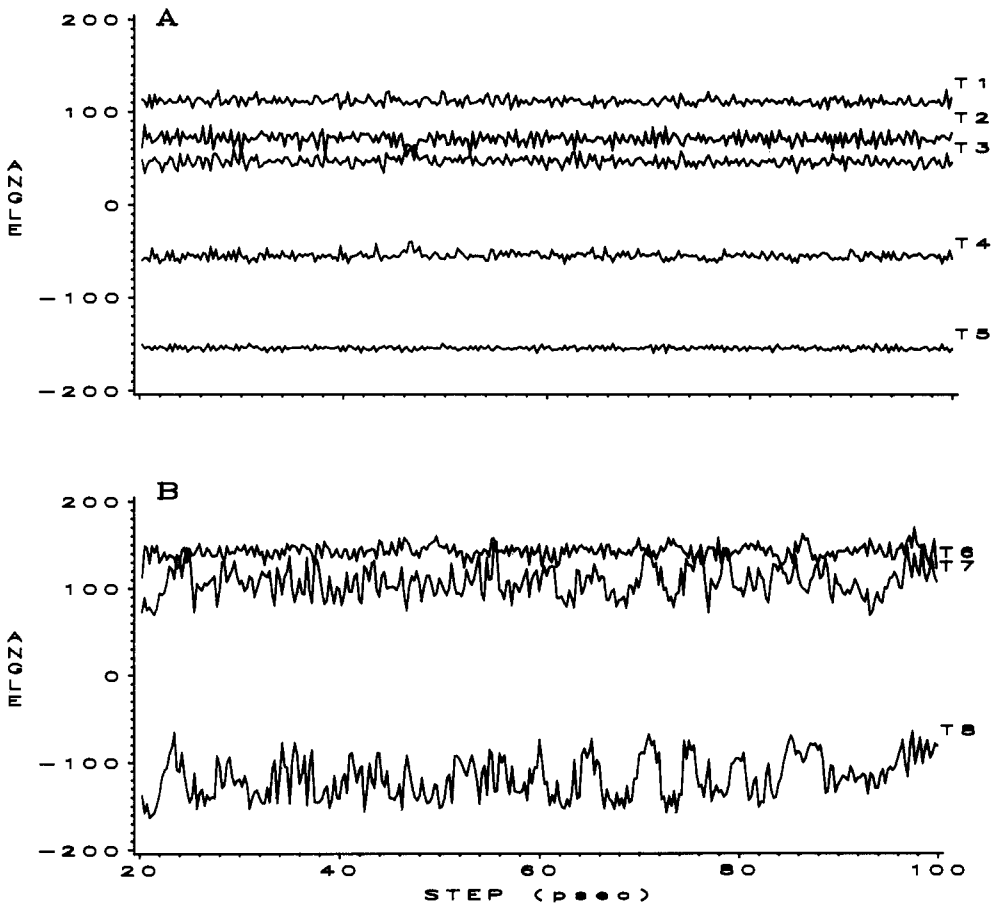

FIGURE 9: Representative dihedral angles of the cyclic peptide as a function of time in the molecular dynamics trajectory at 300 K. (A) Macrocyclic ring [T1 = C4–O, T2 = Cα(Ala)–CO, T3 = Cα(Ala)–N, T4 = C5–C4, T5 = C3–O]. (B) Noncyclic portion of the molecule [T6 = Cα(Val)–CO, T7 = Cα(Ile)–CO, T8 = Cα(His)–N].

experimentally. These data along with the large values observed for some of the J couplings (1b–2a, 2b–3b, 4b–5, ring NH-5) of the macrocyclic ring provided further evidence that the ring is relatively rigid. From a comparison of dihedral angles of the noncyclic portion of the molecule obtained from the dynamics run (e.g., 5–6), one might conclude that the dynamics at 800 K more closely mimics the NMR data. However, as indicated above, the average structural parameters generated from any of the molecular dynamics calculations should not be expected to quantitatively compare to the NMR data.

Conclusions

By obtaining many accurate proton–proton distances from a quantitative analysis of 2D NOE data and dihedral angles from vicinal spin–spin coupling constants, three-dimensional structures of the constrained cyclic peptide were constructed by using several different molecular modeling techniques. The structures consisted of a stable conformation of the macrocyclic ring and a cis Phe–Ala peptide bond. Although all of the modeling techniques investigated were able to predict structures that agreed with the NMR data, they each had their own advantages and disadvantages. The method of interactively rotating about the covalent bonds of the molecule to fit the NMR-determined distance constraints was successful in generating a structure but was found to be tedious, time consuming, and biased by user interaction. The three methods based on an energy minimization criteria (i.e., energy minimization, constrained energy minimization, and constrained molecular dynamics) required less user interactions but tended to get stuck in local minima. Of the three methods, constrained dynamics was clearly superior since it was the least sensitive to the choice of starting structure. For larger molecules, however, this method has been reported to fail due to the large energy barrier between the starting structure and the final structure (Zuiderweg et al., 1985). Another method, distance geometry, which has the advantage of being able to predict structures based solely on the covalent bonding of the molecule and on the NMR distance constraints, has the disadvantage of predicting structures which are energetically unfavorable. For the cyclic peptide, this was remedied by simply applying an energy minimization routine. However, in some cases, this may result in structures which no longer satisfy all of the NMR constraints, and more convergent methods (e.g., constrained molecular dynamics) may be necessary to optimize the structures created from distance geometry.

In order to predict regions of the molecule most likely to be influenced by motional averaging, a molecular dynamics trajectory of the cyclic peptide was analyzed. The distance and angular fluctuations in the cyclic portion of the molecule were very small (i.e., root mean square fluctuations of less than 0.15 Å). These results combined with the NMR data (large J couplings) indicated that a change in the ring pucker of the cyclic portion of the molecule is unlikely. Other regions of the molecule exhibited much larger fluctuations which suggested that the NMR data for these portions of the molecule should not be interpreted in terms of a single static structure.

From the conformational information gained from this work, we attempted to explain the inability of the cyclic peptide to inhibit renin compared to a straight-chain analogue. A model of the cyclic peptide containing the proper conformation of the macrocyclic ring and a cis Phe–Ala peptide bond (C1) was

docked into a computer-generated model of the active site of human renin. In this conformation, the cyclic peptide would not fit into the active site. Different conformations of the cyclic peptide were generated that varied in the noncyclic portion of the peptide where the molecular dynamics calculations suggested flexibility. However, as will be described in detail elsewhere (Sham et al., to be published), none of these structures would fit into the active site. On the basis of the bad contacts observed, it appeared that the cis Phe–Ala peptide bond was the cause of the bad fit. Indeed, analogues of **1** possessing a larger macrocyclic ring (12 or 14 members) displayed an increased population of the trans Phe–Ala peptide bond as determined from NMR and were found to inhibit human renin.

ACKNOWLEDGMENTS

We thank E. R. P. Zuiderweg for writing the 2D base-line correction routine used in the data processing and for many useful discussions.

REFERENCES

Almquist, R. G., Jenning-White, C., Chao, W., Steeger, T., Wheeler, K., Rogers, J., & Mitona, C. (1985) *J. Med. Chem. 28*, 1062.

Andreeva, N. S., Zdanov, A. S., Gustchina, A. E., & Fedorov, A. A. (1984) *J. Biol. Chem. 259*, 11353.

Aue, W. P., Bartholdi, E., & Ernst, R. R. (1976) *J. Chem. Phys. 64*, 2229.

Boger, J., Lohr, N. S., Ulm, E. H., Poe, M., Blaine, E. H., Fanelli, G. M., Lin, T.-Y., Payne, L. S., Schorn, T. W., LaMont, B. I., Vassil, T. C., Stabilito, I. I., Veber, D. F., Rich, D. H., & Bopari, A. S. (1983) *Nature (London) 303*, 81.

Boger, J., Payne, L. S., Perlow, D. S., Lohr, N. S., Poe, M., Blaine, E. H., Ulm, E. H., Schorn, T. W., LaMont, B. I., Lin, T.-Y., Kawai, M., Rich, D. H., & Veber, D. F. (1985) *J. Med. Chem. 28*, 1779.

Bott, R., Subramanian, E., & Davies, D. R. (1982) *Biochemistry 21*, 6956.

Bremer, J., Mendz, G. L., & Moore, W. J. (1984) *J. Am. Chem. Soc. 106*, 4691.

Bystrov, V. F. (1976) *Prog. Nucl. Magn. Reson. Spectrosc. 10*, 41.

Clore, G. M., Gronenborn, A. M., Brünger, A. T., & Karplus, M. (1985) *J. Mol. Biol. 186*, 435.

Feldmann, R., Bing, D. H., Potter, M., Mainhart, C., Furie, B., Furie, B. C., & Caporale, L. H. (1985) *Ann. N.Y. Acad. Sci. 439*, 12.

Fesik, S. W., O'Donnell, T. J., Gampe, R. T., Jr., & Olejniczak, E. T. (1986) *J. Am. Chem. Soc. 108*, 3165.

Greer, J. (1981) *J. Mol. Biol. 153*, 1027.

Greer, J. (1985) *Science (Washington, D.C.) 228*, 1055.

Hagler, A. T. (1985) *Peptides (3rd Ed.) 7*, 213.

Hagler, A. T., Stern, P. S., Sharon, R., Becker, J. M., & Naider, F. (1979) *J. Am. Chem. Soc. 101*, 6842.

Hagler, A. T., Osguthorpe, D. J., Dauber-Osguthorpe, P., & Hempel, J. C. (1985) *Science (Washington, D.C.) 227*, 1309.

Havel, T. F., & Wüthrich, K. (1985) *J. Mol. Biol. 182*, 281.

Havel, T. F., Kuntz, I. D., & Crippen, G. M. (1983) *Bull. Math. Biol. 45*, 665.

James, M. N. G., & Sielecki, A. R. (1983) *J. Mol. Biol. 163*, 299.

Kaptein, R., Zuiderweg, E. R. P., Scheek, R. M., Boelens, R., & van Gunsteren, W. F. (1985) *J. Mol. Biol. 182*, 179.

Lifson, S., Hagler, A. T., & Dauber, P. J. (1979) *J. Am. Chem. Soc. 101*, 5111.

Macura, S., Wüthrich, K., & Ernst, R. R. (1982) *J. Magn. Reson. 47*, 351.

Noggle, J. H., & Shirmer, R. E. (1971) *The Nuclear Overhauser Effect, Chemical Applications*, Academic Press, New York.

Olejniczak, E. T., Gampe, R. T., Jr., & Fesik, S. W. (1986) *J. Magn. Reson. 67*, 28.

Peach, M. J. (1977) *Physiol. Rev. 57*, 313.

Pearl, L., & Blundell, T. (1984) *FEBS Lett. 174*, 96.

Perrin, C. L., & Gipe, R. K. (1984) *J. Am. Chem. Soc. 106*, 4036.

Plattner, J. J., Greer, J., Fung, A. K. L., Stein, H., Kleinert, H. D., Sham, H. L., Smital, J. R., & Perun, T. J. (1986) *Biochem. Biophys. Res. Commun. 139*, 982.

States, D. J., Haberkorn, R. A., & Ruben, D. J. (1982) *J. Magn. Reson. 48*, 286.

Szelke, M., Leckie, B., Hallett, A., Jones, D. M., Sueiras, J., Atrash, B., & Lever, A. F. (1982) *Nature (London) 299*, 555.

Williamson, M. P., Havel, T. F., & Wüthrich, K. (1985) *J. Mol. Biol. 182*, 295.

Zuiderweg, E. R. P., Scheek, R. M., Boelens, R., van Gunsteren, W. F., & Kaptein, R. (1985) *Biochimie 67*, 707.